

# Enhanced Hot Carrier Up-Conversion in Graphene By Quantum Dot Coating

He Ma, Nianze Shang, Jing Liang, Chang Liu, Fangfang Wang, Mengze Zhao, Zhibin Zhang, Zhihong Zhang, Chaojie Ma, Can Liu, Muhong Wu, Huaibin Shen,\* Hao Hong,\* and Kaihui Liu\*

Graphene with unique linear band structure and enhanced electron–electron interaction exhibits peculiar hot-carrier generation. The thermalized hot carriers in graphene have potential to achieve high energy which is well above energy of the incident photons. Together with its outstanding optical and electrical properties, the exotic thermalization of hot carriers makes graphene a promising material for applications in optical up-conversion devices and ultrafast photonics. However, the excitation efficiency of hot carriers is limited by its weak absorption and atomically thin light–matter interaction length. Here, the efficient hot-carrier amplification is demonstrated in graphene by adjacent quantum dots (QD). With pump–probe experiments, this hot carrier amplification is found to stem from the charge collection of the two-photon excited hot carriers in QD. Taking advantages of strong absorption of QD, the hot-carrier excitation efficiency of graphene can be efficiently improved under near-infrared sub-bandgap excitation of QD. The transferred hot carriers are with energy higher than those originally excited in graphene, leading to raised hot-carrier temperature and enhanced hot-carrier up-conversion. This research demonstrates QD's immense potential to realize high efficiency hot-carrier injection in graphene-based devices, which will promote their ability for hot-carrier-driven devices, optical up-conversion devices and high-frequency optoelectronics.

## 1. Introduction

Hot carriers refer to nonequilibrium electrons (or holes) at excited states with large kinetic energy to reach effective elevated temperature.<sup>[1]</sup> Such carriers with high particle temperature play an essential role in the research of excited states dynamics and physics of solid state devices.<sup>[2]</sup> The rise of graphene opens up new horizons and opportunities to the field of hot carrier dynamics and light-harvesting devices. Due to the unique linear-dispersion band structure and rapid electron-electron scattering assisted by Coulomb interactions, hot carriers in graphene can rapidly thermalize to a Fermi–Dirac distribution in which the long tail can extend to energy much higher than the incident photon energy, which is promising for optical up-conversion.<sup>[3,4]</sup> Meanwhile, the thermalization process of hot carriers is as short as tens of femtoseconds and is considered to have great potential for ultrahigh frequency optoelectronic devices.<sup>[5,6]</sup> Those intriguing hot carrier properties, together

H. Ma, N. Shang  
State Key Laboratory for Mesoscopic Physics  
Frontiers Science Center for Nano-optoelectronics  
School of Physics  
Academy for Advanced Interdisciplinary Studies  
Peking University  
Beijing 100871, China

J. Liang, M. Zhao, Z. Zhang, C. Ma, C. Liu  
State Key Laboratory for Mesoscopic Physics  
Frontiers Science Center for Nano-optoelectronics  
School of Physics  
Peking University  
Beijing 100871, China

C. Liu, Z. Zhang, M. Wu  
International Centre for Quantum Materials  
Collaborative Innovation Centre of Quantum Matter  
Peking University  
Beijing 100871, China

F. Wang, H. Shen  
Key Laboratory for Special Functional Materials of Ministry of Education  
School of Materials and Engineering  
Henan University  
Kaifeng 475001, China  
E-mail: shenhuaibin@henu.edu.cn

H. Hong  
State Key Laboratory for Mesoscopic Physics  
Frontiers Science Center for Nano-optoelectronics  
School of Physics  
Interdisciplinary Institute of Light-Element Quantum Materials  
and Research Center for Light-Element Advanced Materials  
Peking University  
Beijing 100871, China  
E-mail: haohong@pku.edu.cn

K. Liu  
State Key Laboratory for Mesoscopic Physics  
Frontiers Science Center for Nano-optoelectronics  
School of Physics  
International Centre for Quantum Materials  
Collaborative Innovation Centre of Quantum Matter  
Academy for Advanced Interdisciplinary Studies  
Peking University  
Beijing 100871, China  
E-mail: khliu@pku.edu.cn

 The ORCID identification number(s) for the author(s) of this article can be found under <https://doi.org/10.1002/adom.202101563>.

DOI: 10.1002/adom.202101563

with the high mobility, broadband absorption, and wide-range photon–electron conversion, make graphene an excellent candidate to the research of optical up-conversion devices and high-frequency optoelectronics.<sup>[7–11]</sup> Thoroughly understanding and efficiently manipulating the behavior of hot carriers in graphene will lead us to higher efficiency, better performances, and brand-new design of relevant optoelectronic and ultrafast photonic devices mentioned above.<sup>[12–14]</sup> However, such utilizations are severely hindered by the weak light–matter interaction of graphene due to its limited thickness.

One plausible way to gain homogenous enhancement of hot carrier excitation in graphene is by hot carrier collection from adjacent medium.<sup>[15–20]</sup> So far, great efforts have been devoted to coupling graphene with semiconductors to acquire stronger light absorbance and efficient hot carrier injection.<sup>[21–31]</sup> Atomically thin graphene–transition metal dichalcogenide (TMDC) heterostructure has been most studied. In MoS<sub>2</sub>/graphene, nondissipative hot carrier transfer from MoS<sub>2</sub> to graphene was proved.<sup>[27]</sup> In addition, the extraction efficiency of C-exciton hot carriers in MoS<sub>2</sub> was confirmed to be about 80% at room temperature.<sup>[32]</sup> An ultrafast selective charge transfer to graphene was detected under resonant excitation of A-exciton in WS<sub>2</sub>,<sup>[28]</sup> and electron injection from PtSe<sub>2</sub> to graphene induced by effective electric field was also recently demonstrated.<sup>[33]</sup> Moreover, other semiconductors such as organic–inorganic halide perovskite (CH<sub>3</sub>NH<sub>3</sub>PbI<sub>3</sub>), QD and GaAs can also provide efficient hot carrier injection to graphene.<sup>[19,34,35]</sup> However, those researches to date are confined to resonant or above bandgap excitation. By contrast, hot carrier injection under sub-bandgap excitation, which has the potential to break the bandgap limitation of adjacent semiconductors and largely extend the photon energy response range, is more appealing but still has not been realized.

In this work, we report efficient hot carrier amplification in QD/graphene (QD/Gr) heterostructure induced by the ultrafast

hot carrier transfer under sub-bandgap excitation of QD. With time-resolved experiments, we found that photogenerated hot carriers of QD are directly extracted by graphene from high-energy excited states before phonon-assisted cooling process. The collected hot carriers lead to notably raised carrier temperature and enhanced carrier up-conversion process in graphene. An over five times hot carrier excitation enhancement of graphene is obtained, with an ultrafast hot carrier transfer time-scale less than 50 fs. Our research provides new evidence to the ultrafast hot carrier transfer process occurring between carrier donors and graphene.

## 2. Results and Discussion

In our experiment, graphene monolayers were prepared by mechanical exfoliation on 90 nm SiO<sub>2</sub>/Si substrates, and CdSe/ZnS core–shell QDs with oleic acid ligands were then spin-coated onto substrates with graphene monolayers (**Figure 1a**). **Figure 1b** shows the optical image of a graphene monolayer with colloidal QD coated on the surface. The absorption and PL spectra of the QD are shown in **Figure 1c**. The PL peak of QD is centered at 620 nm, and the absorption edge is located at about 650 nm. We then measured the two-photon-absorption-induced photoluminescence (TPPL) spectrum of solely QD and the QD/Gr heterostructure under excitation at 820 nm (fluence at 2.77 μJ cm<sup>-2</sup>) (**Figure 1d**). The intensity of QD's TPPL was evidently quenched in the QD/Gr heterostructure, which indicates the electronic coupling and charge transfer process between QD and graphene. **Figure 1e** shows the TPPL mapping corresponding to the QD/Gr heterostructure sample shown in **Figure 1b**, in which the prominent and uniform PL intensity quenching in the heterostructure area confirms the efficient charge transfer between QD and graphene. We further

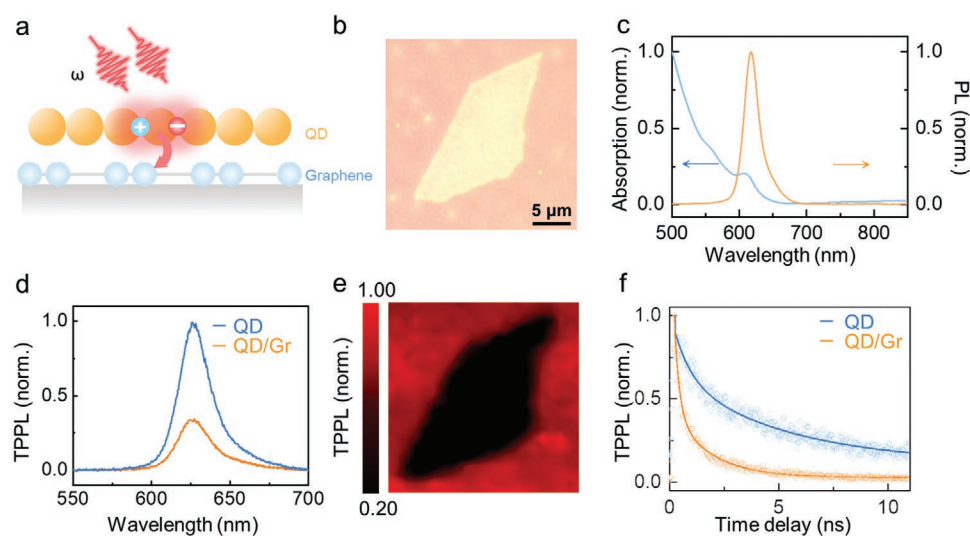


**Figure 1.** Schematic and spectral characterization of QD/graphene heterostructure. a) Schematic representation of QD/graphene (QD/Gr) heterostructure under pulse laser excitation. b) Optical image of the QD/Gr heterostructure, with QD spin-coating on monolayer graphene. c) Absorption (blue) and PL (orange) spectrum of CdSe/ZnS QD. d) Two-photon-absorption-induced photoluminescence (TPPL) spectra of QD and QD/Gr heterostructure under 820 nm excitation (fluence at 2.77 μJ cm<sup>-2</sup>). TPPL intensity of QD quenches to about 30% with graphene underneath. e) TPPL mapping of QD with and without graphene, showing a uniform PL quenching contrast. f) Time-resolved TPPL of QD and QD/Gr heterostructure with lifetime of 2.93 ns and 0.81 ns, respectively.

employed time-resolved TPPL measurements to characterize the carrier dynamics in solely QD and the QD/Gr heterostructure (Figure 1f). A faster relaxation rate was revealed in the heterostructure compared with QD. The photocarrier recombination lifetime  $\tau_0$  in QD is  $\approx 2.93$  ns while in the heterostructure the lifetime  $\tau_1$  reduces significantly to 0.81 ns, which indicates the carrier injection from QD to graphene. By the equation  $\eta = 1 - \frac{\tau_1}{\tau_0}$ , the charge collection efficiency  $\eta$  of the interface can be estimated to be about 72%.<sup>[19]</sup> The carrier extraction from QD to graphene greatly reduced the carrier lifetime of QD.

To capture the ultrafast dynamics of the hot carriers, we employed pump-probe spectroscopy measurement. In the experiment, pump excitation centered at 820 nm with corresponding pump fluence ranging from 0.12 to 1.18  $\mu\text{J cm}^{-2}$ , and the probe pulse was at 700 nm (Figure 2a). The photon energy of the probe beam is higher than that of the pump beam, therefore the pump-induced change directly reflects the dynamics of carriers which populate the band above initial photoexcitation, that is, the hot carrier up-conversion. The transient differential reflection signal  $\frac{\Delta R}{R}$  is measured as a function of delay time. In the reflective configuration, the sample absorption change  $\Delta A$  is given by the reflection change  $-\frac{\Delta R}{R}$ , thus we can directly detect the transient absorption change from the transient differential reflection signal in the experiment. In monolayer graphene, the optical absorption originates from two processes: intraband transition and interband transition. The interband transition is the transition between valence band and conduction band while the intraband transition is the transition within the conduction (valence) band assisted by phonons. The relative contribution of these processes varies with electronic temperature

in the visible and near-infrared spectral range.<sup>[36]</sup> In particular, the intraband (interband) transition plays the leading role at low (high) electronic temperatures. The absorption change of graphene is determined by the real part of optical conductivity,  $\Delta\sigma^{(1)} = \Delta\sigma_{\text{intra}}^{(1)} + \Delta\sigma_{\text{inter}}^{(1)}$ , following the relation:  $\Delta A = \frac{4\pi}{c} \Delta\sigma^{(1)}$ . The intraband and interband contributions of real part of the optical conductivity are represented as<sup>[36–38]</sup>

$$\sigma_{\text{intra}}^{(1)} = \frac{8 \ln 2 \pi e^2}{\pi} \frac{\Gamma k_B T}{2h (\hbar\omega)^2 + \Gamma^2} \quad (1)$$

$$\sigma_{\text{inter}}^{(1)} = \frac{\pi e^2}{2h} \tan h \left( \frac{\hbar\omega}{4k_B T} \right) \quad (2)$$

where  $\hbar\omega$ ,  $T$ , and  $\Gamma$  separately refer to the probe photon energy, electronic temperature, and the scattering rate. According to the temperature-dependence of intraband and interband term, when electronic temperature increases, intraband/interband transition gives rise to positive/negative transient absorption change, respectively. In visible and infrared range, the intraband transition term roughly scales linearly while interband transition term varies approximately exponentially to the electronic temperature  $T$ . Therefore, the ultrafast nonequilibrium dynamics of photocarriers in graphene is strongly correlated with the pump fluence.<sup>[39]</sup> Comparing different temporal evolution behavior, we are able to determine the dominate transition process in graphene and deduce the relative electronic temperature. Consistent with previous reports,<sup>[36,40]</sup> the transient absorption evolution of hot carriers in graphene experiences a crossover from positive to negative absorption change with the increase of pump fluence (Figure 2b).

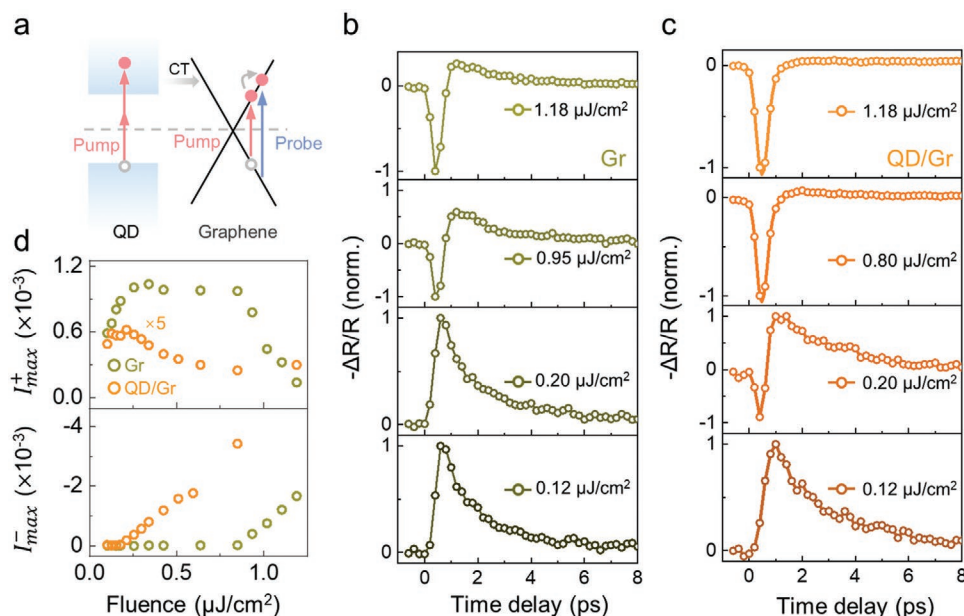


**Figure 2.** Hot carrier transfer in the heterostructure. a) Schematic of band alignment and photocarrier transfer in the QD/Gr heterostructure. Thick gray arrow refers to carrier transfer (CT) process from QD to graphene. b) Transient absorption dynamics of pristine graphene at different pump fluence from 0.12 to 1.18  $\mu\text{J cm}^{-2}$ , the peaks near time-zero undergo a transition from intraband dominated absorption (positive  $I_{\text{max}}^+$ ) to interband dominated bleaching (negative  $I_{\text{max}}^-$ ). c) Transient absorption dynamics of QD/Gr heterostructure at different pump fluence. The transition is similar to pristine Gr, while the interband dominated bleaching occurs at lower pump fluence. d) The magnitude of  $I_{\text{max}}^+$  and  $I_{\text{max}}^-$  at different pump fluence.

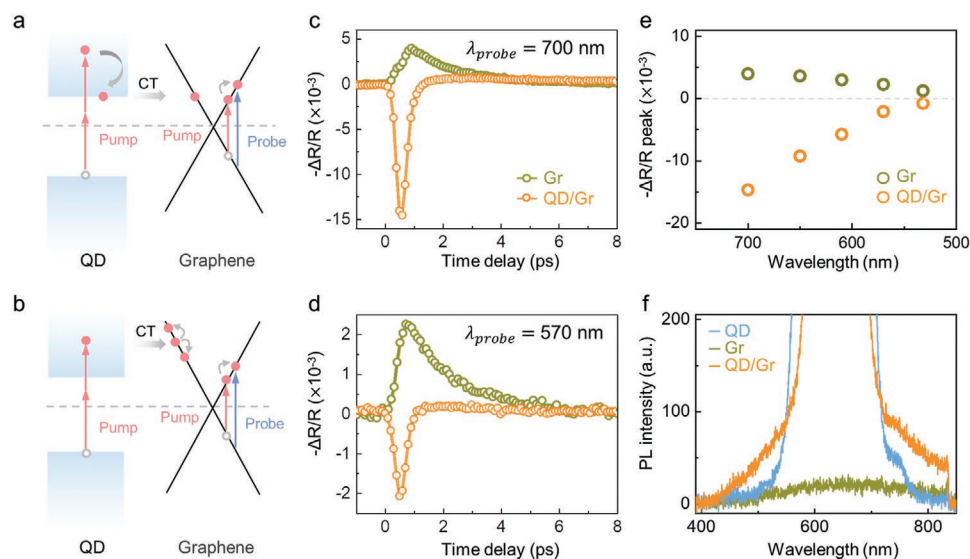


**Figure 3.** Broadband hot carrier enhancement in the QD/Gr heterostructure. a,b) Schematic of two different carrier transfer channels from QD to Gr: (a) transfer after cooling to band edges and (b) direct hot carrier transfer. Thick gray arrow refers to carrier transfer (CT) process from QD to graphene and thin gray arrow refers to the carrier redistribution process in graphene. c,d) Evolution of transient absorption dynamics of pristine graphene and QD/Gr heterostructure under pump wavelength at 820 nm and probe wavelength at (c) 700 nm and (d) 570 nm. In a wide probe energy range, the transient absorption changes of pristine graphene remain positive and the transient absorption changes of the QD/Gr heterostructure are all negative in sign. e) Peak intensity of transient absorption dynamics of pristine graphene and QD/Gr heterostructure under different probe wavelength from 532 to 700 nm. f) Emission spectra of QD, pristine graphene and QD/Gr heterostructure under excitation at 910 nm. A wide spectral range enhancement of graphene's ultrafast PL can be observed in QD/Gr heterostructure.

In our pump fluence range ( $0.12\text{--}1.18 \mu\text{J cm}^{-2}$ ), the QD/Gr heterostructure exhibits similar temporal evolution trend as monolayer graphene, i.e., the transient absorption changes from positive to negative with increasing pump fluence. However, the negative absorption peak in heterostructure appears at a much lower pump fluence than in graphene (Figure 2c). We extract the positive and negative transient absorption peak amplitude from the fluence-dependent experiment, defining the maximal positive and negative transient absorption signal as  $I_{\text{max}}^+$  and  $I_{\text{max}}^-$ . In monolayer graphene,  $I_{\text{max}}^-$  doesn't appear until pump fluence is above  $0.80 \mu\text{J cm}^{-2}$ . By contrast, it only requires about  $0.13 \mu\text{J cm}^{-2}$  in the heterostructure (Figure 2d) to reach this transition point. Given the transient absorption of graphene is strongly electronic temperature dependent, the emergence of negative peak corresponds to the critical electronic temperature that intraband transition is exceeded by the interband transition. Therefore, we can conclude that the hot carrier excitation efficiency in graphene is improved up to five times after coated by QD under small pump fluence near the intra-interband transition critical point. We attribute the enhanced hot carrier excitation in graphene to photogenerated carrier transferring from adjacent QD. Due to strong light absorption of QD, this carrier injection is highly efficient compared to original carrier excitation in graphene. By contrast, no time-resolved pump-probe signal can be observed in solely QD under our experimental conditions.

Since the pump photon energy (at 820 nm) in our experiment is smaller than the bandgap of CdSe/ZnS QD (620 nm), two photons are required to realize the excitation of QD. There are two potential routes for carriers in CdSe/ZnS QD transferring to graphene: the photoexcited carriers in QD can (1) relax

to the band edges through phonon-assisted cooling before collected by graphene, or (2) directly transfer to graphene from the excited states, that is, hot-carrier transfer.<sup>[41,42]</sup> For the after-cooling transfer process, the carriers collected by graphene relax to QD's band edges first and give rise to limited redistribution in graphene (Figure 3a). The Fermi level of graphene locates at about  $E_F = -4.58 \text{ eV}$ <sup>[43,44]</sup> (Figure S1a–e, Supporting Information). The highest occupied molecular orbital (HOMO) and lowest unoccupied molecular orbital (LUMO) of CdSe/ZnS QD are  $E_H = -5.88 \text{ eV}$  and  $E_L = -3.89 \text{ eV}$ , respectively (Figure S1f, Supporting Information). Thus, the estimated energy barrier  $E_B$  between HOMO of CdSe/ZnS QD and graphene Fermi level is  $\approx 0.73 \text{ eV}$ . If photocarriers in QD transfer to graphene layers after relaxing to the band edges, the excitation enhancement range will not exceed  $2E_B \approx 1.46 \text{ eV}$ . While for the hot carrier transfer process, the hot carriers will go through thermal equilibrating redistribution, leading to extended density of states (to higher energy states) in the linear band structure of graphene (Figure 3b). To figure out the underlying mechanism, we measured the probe wavelength-dependent transient absorption spectroscopy at fixed pump fluence  $\approx 0.60 \mu\text{J cm}^{-2}$ . As probe wavelength varies from 700 to 532 nm (Figure 3c,d), the transient absorption changes of graphene are all positive in sign, which means intraband transition is always dominated in graphene. On the contrary, the optical responses all reverse to negative in QD/Gr heterostructure at whole probe range. The significant changes reflect that within the probe range, the optical responses in the heterostructure are all dominated by the interband transition with higher electronic temperature, which suggests that hot carrier excitation in our probing range are always enhanced (Figure 3e). Relaxation time in pristine graphene is

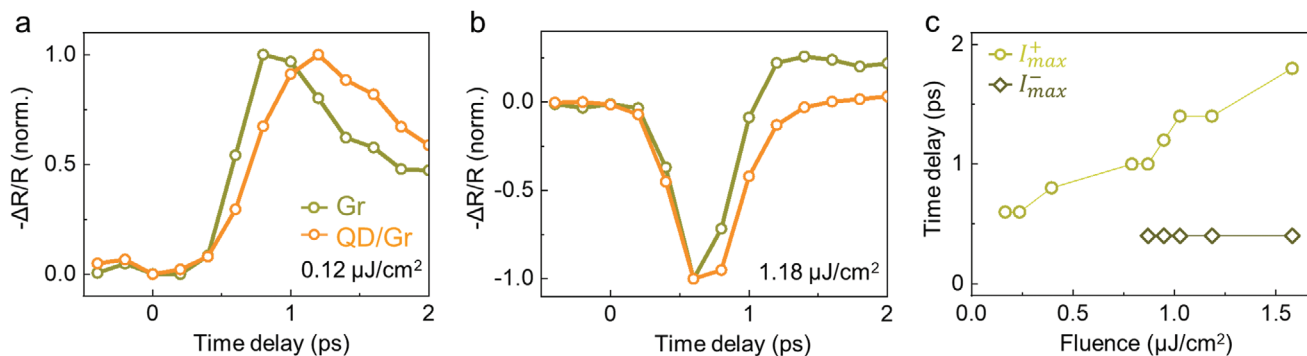


**Figure 4.** Ultrafast hot carrier transfer in the QD/Gr heterostructure. a,b) Rising-up curves of transient absorption dynamics when graphene and QD/Gr heterostructure are both dominated by (a) intraband transition (pumped at  $0.12 \mu\text{J}/\text{cm}^2$ ) and (b) interband transition (pumped at  $1.18 \mu\text{J}/\text{cm}^2$ ). When intraband transition dominates, a longer rising edge occurs in the QD/Gr heterostructure. By contrast, no difference in rising edge delay can be seen when interband transition dominates, indicating the ultrafast (less than 50 fs) hot carrier transfer process. c) The delay time of  $I_{\text{max}}^+$  and  $I_{\text{max}}^-$  of pristine Gr at different pump fluence.

longer than QD/Gr heterostructure because of inefficient electron-optical phonon cooling resulting from weak excitation.<sup>[45]</sup>

The amplified hot carriers potentially boost the optical response of graphene. Although graphene is a zero-bandgap semimetal of which the PL process is supposed to be suppressed, the thermalized hot carriers in graphene facilitate to realize ultrafast PL emission when excited by femtosecond laser.<sup>[8,9]</sup> The ultrafast PL signal resulting from hot carriers shows wide range emission spectrum from photon energies above the pump photons. Under femtosecond pulse laser excitation at 910 nm ( $1.36 \text{ eV}$ ,  $6.42 \mu\text{J}/\text{cm}^2$ ), the ultrafast PL spectrum of pristine graphene and QD/Gr heterostructure are shown in Figure 3f. Compared to solely QD, the TPPL signal of QD in the heterostructure is rapidly quenched. Meanwhile, out of QD TPPL spectral range, at 430–550 and 700–842 nm (842 nm corresponding to the cut-off wavelength of the filter), the signal intensity in heterostructure evidently increases compared with isolated graphene and QD. Since the enhancement covers wide spectral range without characteristic sharp peaks, it can only be attributed to the enhanced ultrafast upconverted PL signal of graphene. We note that, population of carriers with energy both larger (430–550 nm) and smaller (700–842 nm) than the bandgap of QD (at 620 nm) are boosted, which is consistent with the physical picture as shown in Figure 3b. Also, besides the intensity enhancement, the starting wavelength of ultrafast PL in heterostructure (at 430 nm) is much shorter than in pristine graphene (at 500 nm), indicating that the transferred carriers from QD host higher kinetic energy than those originally excited in graphene and are active in redistribution and multiplication process.

We then compared the difference between the transient absorption dynamics of pristine graphene and the QD/Gr heterostructure in different excitation regime to find out the charge transfer dynamics in the heterostructure (extracted from Figure 2b,c). In the case of both graphene and heterostructure dominated by intraband transition, featuring positive transient absorption change (fluence of  $0.12 \mu\text{J}/\text{cm}^2$ ), the rising-up curve (by deconvolution of the transient absorption signal) of heterostructure ( $\approx 360 \text{ fs}$ ) is about 260 fs longer than in graphene ( $\approx 100 \text{ fs}$ ). By contrast, when the optical response is predominantly depended by Pauli blocking induced by interband transition,

the rising-up curve of the heterostructure is the same as that of graphene (fluence of  $1.18 \mu\text{J}/\text{cm}^2$ ) (Figure 4a,b). The difference can be traced back to the contribution ratio of intraband transition and interband transition.<sup>[39,46]</sup> Figure 4c shows the fluence dependence of the time-delay linked to  $I_{\text{max}}^+$  and  $I_{\text{max}}^-$  (if any) in pristine graphene. The time-delay of  $I_{\text{max}}^+$  gets larger with increasing fluence. Since the increasing pump fluence leads to more efficient Pauli blocking induced by interband transition, it gives rise to a stronger bleaching which actually cancels out the positive peak amplitude at the early time and leads to  $I_{\text{max}}^+$  occur at longer time-delay.<sup>[39]</sup> Hence the longer rising-up curves of  $I_{\text{max}}^+$  in heterostructure prove the hot carrier excitation efficiency is improved. When it comes to interband transition, the redistribution of thermalized hot carriers is established in very short timescales, and the rising-up curves of  $I_{\text{max}}^-$  give no apparent fluence-dependence. There is no temporal variation only amplitude enhancement in the rising-up curve of heterostructure at the interband transition dominated regime, which indicates the time scale of hot carrier transfer in the QD/Gr heterostructure is ultrafast within our temporal resolution. In addition, the charge transfer time should be comparably ultrafast with the ultrafast PL emission process in graphene, which can then boost intensity of the latter. Given that the ultrafast PL emission in graphene is in time scale of tens of femtoseconds,<sup>[8,9]</sup> the ultrafast hot carrier transfer process should be on a time scale shorter than 50 fs.

### 3. Conclusion

In summary, we have investigated the excitation enhancement of the hot carriers in graphene by ultrafast hot carrier transfer from adjacent CdSe/ZnS QD. Under sub-bandgap excitation, two-photon excited hot carriers in QD would directly transfer to graphene within 50 fs. The transferred carriers are with higher kinetic energy than those in graphene, which will take part into the ultrafast thermal redistribution and multiplication process, leading to notable hot carrier up-conversion and boost the hot carrier excitation efficiency by up to 5 times under small pump fluence. Our research paves a new way for hot carrier collection, which will facilitate the development of graphene-based

hot carrier-driven high-frequency optoelectronics, light-harvesting and near-infrared detection devices.

## 4. Experimental Section

**Transient Absorption Dynamics Measurements:** Ti:sapphire oscillator (Spectra-Physics Mai Tai laser) with femtosecond pulses ( $\approx 100$  fs, 80 MHz) and an optical parametric amplifier (OPO) were used to perform the pump–probe transient absorption dynamics measurements. The wavelength of pump/probe was 820 nm / 532–700 nm, respectively. The pump–probe time delay was controlled by a motorized delay stage. The probe beam was focused onto the sample by an objective (40x, N.A. = 0.65) and detected by a photomultiplier tube (PMT) with reflective geometry. 750 nm short-pass filter was used to filter out the pump pulse.

**Time-Resolved PL Spectroscopy:** Pulse from Ti:sapphire oscillator at 820 nm was used to excite samples. The PL signal of target wavelength was selected at 620 nm by a 750 nm short-pass filter and a spectrometer (with resolution of  $\approx 2$  nm) after photoexcitation and collection. Then, the time-resolved PL signal was acquired using single-photon APD (PicoQuant Company, TDA 200) combining with a TCSPC module (TimeHarp 260 PICO Single). The integral time was set as 1 s with pump fluence at  $2.77 \mu\text{J cm}^{-2}$ .

**Ultrafast PL Spectra:** Femtosecond pulse laser at 910 nm ( $\approx 100$  fs, 80 MHz) is generated by a Ti:sapphire oscillator (Spectra-Physics Mai Tai laser). 842 nm short-pass filter was used to filter out the pump pulse. The integral time was set as 10 s with pump fluence at  $6.42 \mu\text{J cm}^{-2}$ .

## Supporting Information

Supporting Information is available from the Wiley Online Library or from the author.

## Acknowledgements

H.M., N.S., and J.L. contributed equally to this work. K.L., H.H., and H.S. supervised the project. This work was supported by the National Natural Science Foundation of China (52025023, 51991342, 52021006, 11888101), the Key R&D Program of Guangdong Province (2020B010189001, 2019B010931001, 2018B030327001), the Strategic Priority Research Program of Chinese Academy of Sciences (XDB33000000), Beijing Natural Science Foundation (JQ19004), the Pearl River Talent Recruitment Program of Guangdong Province (2019ZT08C321), and China Postdoctoral Science Foundation (2021T140022).

## Conflict of Interest

The authors declare no conflict of interest.

## Data Availability Statement

Research data are not shared.

## Keywords

graphene, hot carriers, up-conversion, charge transfer, quantum dots

Received: July 29, 2021  
Revised: September 19, 2021  
Published online:

- [1] T. Y. Stokoe, J. F. Cornwell, *Phys. Status Solidi B* **1972**, *49*, 209.
- [2] K. K. Paul, J.-H. Kim, Y. H. Lee, *Nat. Rev. Phys.* **2021**, *3*, 178.
- [3] D. Kozawa, Y. Miyauchi, S. Mouri, K. Matsuda, *J. Phys. Chem. Lett.* **2013**, *4*, 2035.
- [4] D. Kozawa, X. Zhu, Y. Miyauchi, S. Mouri, M. Ichida, H. B. Su, K. Matsuda, *J. Phys. Chem. Lett.* **2014**, *5*, 1754.
- [5] S. J. Tan, L. M. Liu, Y. A. Dai, J. D. Ren, J. Zhao, H. Petek, *J. Am. Chem. Soc.* **2017**, *139*, 6160.
- [6] S. J. Tan, A. Argondizzo, C. Wang, X. F. Cui, H. Petek, *Phys. Rev. X* **2017**, *7*, 011004.
- [7] F. Wang, Y. B. Zhang, C. S. Tian, C. Girit, A. Zettl, M. Crommie, Y. R. Shen, *Science* **2008**, *320*, 206.
- [8] W.-T. Liu, S. W. Wu, P. J. Schuck, M. Salmeron, Y. R. Shen, F. Wang, *Phys. Rev. B* **2010**, *82*, 081408.
- [9] C. H. Lui, K. F. Mak, J. Shan, T. F. Heinz, *Phys. Rev. Lett.* **2010**, *105*, 127404.
- [10] D. Sun, G. Aivazian, A. M. Jones, J. S. Ross, W. Yao, D. Cobden, X. Xu, *Nat. Nanotechnol.* **2012**, *7*, 114.
- [11] Z. Zhang, P. Lin, Q. Liao, Z. Kang, H. Si, Y. Zhang, *Adv. Mater.* **2019**, *31*, 1806411.
- [12] S. Kumar, M. Anija, N. Kamaraju, K. S. Vasu, K. S. Subrahmanyam, A. K. Sood, C. N. R. Rao, *Appl. Phys. Lett.* **2009**, *95*, 191911.
- [13] G. Xing, H. Guo, X. Zhang, T. C. Sum, C. H. Huan, *Opt. Express* **2010**, *18*, 4564.
- [14] J. Zhang, J. Schmalian, T. Li, J. Wang, *J. Phys.: Condens. Matter.* **2013**, *25*, 314201.
- [15] E. K. Jeon, C. S. Yang, Y. Shen, T. Nakanishi, D. S. Jeong, J. J. Kim, K. S. Ahn, K. J. Kong, J. O. Lee, *Nanotechnology* **2012**, *23*, 455202.
- [16] Y. Jiang, L. Miao, G. Jiang, Y. Chen, X. Qi, X. F. Jiang, H. Zhang, S. Wen, *Sci. Rep.* **2015**, *5*, 16372.
- [17] K. Liu, Z. H. Zhu, X. J. Li, J. F. Zhang, X. D. Yuan, C. C. Guo, W. Xu, S. Q. Qin, *ACS Photonics* **2015**, *2*, 797.
- [18] G. Froehlicher, E. Lorchat, S. Berciaud, *Phys. Rev. X* **2018**, *8*, 011007.
- [19] H. Hong, J. Zhang, J. Zhang, R. Qiao, F. Yao, Y. Cheng, C. Wu, L. Lin, K. Jia, Y. Zhao, Q. Zhao, P. Gao, J. Xiong, K. Shi, D. Yu, Z. Liu, S. Meng, H. Peng, K. Liu, *J. Am. Chem. Soc.* **2018**, *140*, 14952.
- [20] P. Zereski, M. M. Tavakoli, P. Valencia-Acuna, J.-H. Park, J. Kong, H. Zhao, *Phys. Rev. B* **2019**, *100*, 235411.
- [21] N. Fuyuno, D. Kozawa, Y. Miyauchi, S. Mouri, R. Kitaura, H. Shinohara, T. Yasuda, N. Komatsu, K. Matsuda, *Adv. Opt. Mater.* **2014**, *2*, 983.
- [22] B. Rogez, H. Yan, E. L. Moal, S. Leveque-Fort, E. Boer-Duchemin, F. Yao, Y. H. Lee, Y. Zhang, K. D. Wegner, N. Hildebrandt, A. Mayne, G. Dujardin, *J. Phys. Chem. C* **2014**, *118*, 18445.
- [23] A. Raja, A. Montoya-Castillo, J. Zultak, X. X. Zhang, Z. L. Ye, C. Roquetalet, D. A. Chenet, A. M. van der Zande, P. Huang, S. Jockusch, J. Hone, D. R. Reichman, L. E. Brus, T. F. Heinz, *Nano Lett.* **2016**, *16*, 2328.
- [24] H. M. Zhu, Y. Yang, K. F. Wu, T. Q. Lian, *Annu. Rev. Phys. Chem.* **2016**, *67*, 259.
- [25] Y. Z. Chen, Y. J. Li, Y. D. Zhao, H. Z. Zhou, H. M. Zhu, *Sci. Adv.* **2019**, *5*, eaax9958.
- [26] C. Zhang, L. Lian, Z. Yang, J. Zhang, H. Zhu, *J. Phys. Chem. Lett.* **2019**, *10*, 7665.
- [27] M. D. Tran, S. G. Lee, S. Jeon, S. T. Kim, H. Kim, V. L. Nguyen, S. Adhikari, S. Woo, H. C. Park, Y. Kim, J. H. Kim, Y. H. Lee, *ACS Nano* **2020**, *14*, 13905.
- [28] S. Aeschlimann, A. Rossi, M. Chavez-Cervantes, R. Krause, B. Arnoldi, B. Stadtmuller, M. Aeschlimann, S. Forti, F. Fabbri, C. Coletti, I. Gierz, *Sci. Adv.* **2020**, *6*, eaay0761.
- [29] X. Xing, L. Zhao, W. Zhang, Z. Wang, H. Su, H. Chen, G. Ma, J. Dai, W. Zhang, *Nanoscale* **2020**, *12*, 2498.
- [30] T. G. Park, B. K. Choi, J. Park, J. Kim, Y. J. Chang, F. Rotermund, *ACS Nano* **2021**, *15*, 7756.

- [31] Z. Y. Zhang, M. C. Hu, T. Y. Jia, J. Du, C. Chen, C. W. Wang, Z. Z. Liu, T. C. Shi, J. Tang, Y. X. Leng, *ACS Energy Lett.* **2021**, *6*, 1740.
- [32] L. Wang, Z. Wang, H. Y. Wang, G. Grinblat, Y. L. Huang, D. Wang, X. H. Ye, X. B. Li, Q. L. Bao, A. S. Wee, S. A. Maier, Q. D. Chen, M. L. Zhong, C. W. Qiu, H. B. Sun, *Nat. Commun.* **2017**, *8*, 13906.
- [33] Q. S. Ma, W. J. Zhang, C. W. Wang, R. H. Pu, C. W. Ju, X. Lin, Z. Y. Zhang, W. M. Liu, R. X. Li, *J. Phys. Chem. C* **2021**, *125*, 9296.
- [34] G. Konstantatos, M. Badioli, L. Gaudreau, J. Osmond, M. Bernechea, F. P. G. de Arquer, F. Gatti, F. H. L. Koppens, *Nat. Nanotechnol.* **2012**, *7*, 363.
- [35] J. H. Yang, Q. Sun, W. Liu, Z. B. Zhang, X. Y. Hu, K. H. Liu, H. Yang, H. Misawa, Q. H. Gong, *Adv. Opt. Mater.* **2019**, *7*, 1900580.
- [36] L. M. Malard, K. Fai Mak, A. H. Castro Neto, N. M. R. Peres, T. F. Heinz, *New J. Phys.* **2013**, *15*, 015009.
- [37] K. F. Mak, M. Y. Sfeir, Y. Wu, C. H. Lui, J. A. Misewich, T. F. Heinz, *Phys. Rev. Lett.* **2008**, *101*, 196405.
- [38] K. F. Mak, L. Ju, F. Wang, T. F. Heinz, *Solid State Commun.* **2012**, *152*, 1341.
- [39] K. M. Dani, J. Lee, R. Sharma, A. D. Mohite, C. M. Galande, P. M. Ajayan, A. M. Dattelbaum, H. Htoon, A. J. Taylor, R. P. Prasankumar, *Phys. Rev. B* **2012**, *86*, 125403.
- [40] R. Gatamov, A. Baydin, H. Krzyzanowska, N. Tolk, *Mater. Res. Express* **2020**, *7*, 095601.
- [41] W. A. Tisdale, K. J. Williams, B. A. Timp, D. J. Norris, E. S. Aydil, X. Y. Zhu, *Science* **2010**, *328*, 1543.
- [42] K. Wu, J. Chen, J. R. McBride, T. Lian, *Science* **2015**, *349*, 632.
- [43] S. Larentis, J. R. Tolsma, B. Fallahazad, D. C. Dillen, K. Kim, A. H. MacDonald, E. Tutuc, *Nano Lett.* **2014**, *14*, 2039.
- [44] R. Frisenda, A. J. Molina-Mendoza, T. Mueller, A. Castellanos-Gomez, H. S. J. van der Zant, *Chem. Soc. Rev.* **2018**, *47*, 3339.
- [45] M. Massicotte, G. Soavi, A. Principi, K.-J. Tielrooij, *Nanoscale* **2021**, *13*, 8376.
- [46] F. Kadi, T. Winzer, E. Malic, A. Knorr, F. Göttfert, M. Mittendorff, S. Winnerl, M. Helm, *Phys. Rev. Lett.* **2014**, *113*, 035502.